Biodegradable Polyester Films from Renewable Aleuritic Acid: Surface Modifications Induced by Melt-polycondensation in Air.

José Jesús Benítez[a,*], José Alejandro Heredia-Guerrero[b], María Inmaculada de Vargas-Parody[a], Miguel Angel Cruz-Carrillo[a], Victor Morales-Flórez[c], Nicolás de la Rosa-Fox[d] and Antonio Heredia[e].

[a] Instituto de Ciencia de Materiales de Sevilla, Centro mixto CSIC-Universidad de Sevilla, Americo Vespucio 49, Isla de la Cartuja, 41092-Sevilla (Spain).

e-mail: benitez@icmse.csic.es. phone: 34954489551; fax: 34954460665

[b] Smart Materials, Department of Nanophysics, Fondazione Istituto Italiano di Tecnologia (IIT), via Morego 30, 16163 Genoa (Italy). e-mail: Jose.Guerrero@iit.it

[c] Departamento de Física de la Materia Condensada, Universidad de Sevilla, Avda. Reina Mercedes s/n, 41012 Sevilla (Spain). e-mail: vmorales@us.es

[d] Departamento de Física de la Materia Condensada, Universidad de Cádiz, Avda. República Saharaui s/n, 11510 Puerto Real, Cádiz (Spain). e-mail: nicolas.rosafox@uca.es

[e] Departamento de Biología Molecular y Bioquímica, Universidad de Málaga, 29071 Málaga (Spain). e-mail: heredia@uma.es

* Corresponding author

ABSTRACT

Good water barrier properties and biocompatibility of long-chain biopolyesters like cutin and suberin have potentiated the design of synthetic mimetic materials. Most of these biopolymers are made out esterified mid-chain functionalized ω-long chain hydroxyacids. Aleuritic (9,10,16-trihydroxypalmitic) acid is one of those polyhydroxylated fatty acids and it is also the major constituent of natural lac resin, a relatively abundant and renewable resource. Insoluble and thermostable films have been prepared from aleuritic acid by melt-condensation polymerization in air without using catalysts, an easy and attractive procedure for large scale production. Intended to be used as a protective coating, the barrier performances are expected to be conditioned by the physical and chemical modifications induced by oxygen on the air exposed side. Hence, the chemical composition, texture, mechanical behavior, hydrophobicity, chemical resistance and biodegradation of the film surface have been studied by Attenuated Total Reflection-Fourier Transform Infrared Spectroscopy (ATR-FTIR), Atomic Force Microscopy (AFM), Nanoindentation and Water Contac Angle (WCA). It has been demonstrated that the occurrence of side oxidation reactions conditioned the surface physical and chemical properties of these polyhydroxyester films. Additionally, the addition of palmitic acid to reduce the presence of hydrophilic free hydroxyl groups was found to have a strong influence in these parameters.

Keywords: renewable polyesters, biodegradable long-chain polyesters, films and coatings, polymer surface characterization.

1. **Introduction**

Among renewable polyesters, most of the interest has concentrated on short chain poly(lactic acid) (PLA) and polyhydroxybutyrates (PHBs). Nevertheless, much less attention has been paid to long chain (>C_{16}) homologues, mostly because of the lack of effective and practical routes for monomer obtaining and the difficulties of preparing high molecular weight polyesters by polycondensation. However, long chain biopolyesters like cutin and suberin are widespread in higher plant as protective hydrophobic tissues [1]. The biocompatibility and good barrier properties and of these biopolymers [2] have potentiated the interest in developing mimetic materials, particularly, from the abundant and renewable natural cutin and suberin stock [3,4,5,6,7]. For instance, the *ex situ* reconstruction of waterproof and antimicrobial films from suberin using ionic liquid and the formation of free-standing films from cutin polyhydroxyacids, have been recently reported [8,9].

Cutin, for instance, is an amorphous, insoluble and infusible fatty polyester mostly made out of inter-esterified C_{16} and C_{18} polyhydroxyacids [10,11]. Among them, the midchain hydroxylated ω-hydroxyacids are the most abundant, but there are monomers with other functionalities like unsaturations, epoxy and vicinal diols. This later type of hydroxyacid is of particular interest because it is also present in shellac, a derivate of natural lac resin with applications as non-toxic coatings for wood, pharmaceuticals and food [12]. The major component of shellac is the 9,10,16-trihydroxy palmitic (aleuritic) acid, and, with a global shellac production of about 5000 tons per year and a potential capacity of 50000 tons/year [13], aleuritic acid becomes a non-negligible, accessible and renewable feedstock for synthetic long-chain polyhydroxyesters.

On the other side, the non-toxicity and biodegradability of these biopolymers have driven the applicability of synthetic long chain polyhydroxesters as films and coatings for food packaging, particularly considering the toxicity associated to bisphenol A and phthalates additives. Thus, and to preserve innocuousness, to reduce pollutants and to make the process attractive for large scale production, we have avoided the use organometallic catalysts, aromatic hydrophilic compounds or organic solvents in the synthesis and we have explored the potential of the direct fabrication by melt-condensation polymerization in air without using catalysts [14,15].

In the aleuritic acid molecule the –OH/-COOH ratio is 3 and hence, polyesters derived from this monomer are expected to contain free hydroxyls. Though such hydroxyl phase may compromise the hydrophobicity and the water barrier performances, it may also act as a secondary hydrogen bonded network reinforcing the polymer structure. Thus, aleuritic acid becomes a suitable molecule to investigate these issues as well as the reactivity of the diol moiety under an oxidative atmosphere as the one used in our preparation conditions. In a previous work, we studied polyesters films synthesized from aleuritic and palmitic acid mixtures and we observed that the regulation of the -OH/-COOH imbalance had a strong influence on many bulk properties [15]. However, if conceived as a few microns thick coating layer, as the one used as the internal varnish of food metal containers, the physicochemical properties of the resulting external surface are of key importance since it may condition the barrier performances of the whole coating. For this reason, this article focusses on the physicochemical characterization of the air exposed side of polyhydroxyester films formed by the melt-polycondensation of aleuritic (ALE) and palmitic (PAL) acid mixtures in air without using catalysts.

1. Methods and materials

1.1. Materials

Aleuritic (ALE) (DL-*threo*-9,10,16-trihydroxypalmitic, $C_{16}H_{32}O_5$) acid (93.8% by titration) and palmitic (PAL) ($C_{16}H_{32}O_2$) acid ($\geq$ 99%) were purchased from Fluka. Aleuritic acid was purified by washing with cold deionized water.

1.2. Film preparation

Polyhydroxyester films from aleuritic and palmitic acid mixtures (ALE/PAL = 10/0, 9/1, 8/2, 7/3, 6/4 and 5/5, mol/mol) were prepared by heating the mixture at 150°C in an air convection oven and using an open carbon doped Teflon mold (30 mm x 10 mm and 1 mm deep). Thermogravimetry measurements revealed a significant thermal loss of the palmitic fraction along the synthesis. The weight of the mixture used was then selected to account for such loss and to obtain uniform films thickness of about (350±50) μm. Final products were yellow to light brown and rubbery solid films that were easily removed from the molds. Samples were infusible and quite insoluble in solvents such as chloroform, light alcohols, toluene, tetrahydrofuran, dimethylformamide and dimethyl sulfoxide. Insoluble fractions were determined from sample weight after treating them with dimethyl sulfoxide at 100°C for 24 h.

1.3. Chemical characterization

^{1}H and ^{13}C Cross Polarization Magic Angle Spinning Nuclear Magnetic Resonance Spectroscopy (CP-MAS NMR) spectra of solid samples were recorded on a Bruker Avance III WB 600 MHz spectrometer with 4 mm zirconia rotors spun at magic angle at 10 KHz. Spectra were acquired using a 4.1 μs proton 90º pulse, 2 ms contact time and 2.5 s repetition time. Chemical shifts are referred to tetramethylsilane (TMS).

The chemical composition of the near surface region of films was investigated by Attenuated Total Reflection Fourier Transform Infrared Spectroscopy (ATR-FTIR) using a single reflection ATR accessory (MIRacle ATR, PIKE Technologies) with a diamond crystal. The accessory is mounted on a FTIR spectrometer (JASCO, FT/IR-6200) equipped with a liquid nitrogen cooled Mercury Cadmium Telluride (MCT) detector. Spectra were recorded in the 4000 to 600 cm^{-1} range at 4 cm^{-1} resolution and 50 scans were accumulated. They were processed to account for the penetration depth dependence on the wavelength of the IR beam in ATR. Considering the experimental setup and assuming a sample refractive index (n_2) of 1.5, the effective penetration (d_e) of the IR beam in the single reflection measurement is calculated to about 2.5 μm at λ = 1730 cm^{-1}. For depth profile analysis, a motorized ATR variable angle accessory (Veemax II, PIKE Technologies) with a ZnSe window was used. Incident radiation was polarized perpendicularly to the surface of the sample (p polarization). Effective penetration depth ($d_{e\perp}$) achieved with this experimental setup ranged from 1.7 to 32 μm as calculated from Eq. (1) at λ = 1730 cm^{-1} (carbonyl peak) and n_1 = 2.4 (ZnSe crystal) and n_2 = 1.5 (sample).

$$d_{e\perp} = \frac{n_1^2 n_2 \cos\theta}{(n_1^2 - n_2^2)} \frac{\lambda}{\pi\sqrt{n_1^2 \sin^2\theta - n_2^2}} \quad (1)$$

1.4. Physical characterization

Mechanical properties at the near surface region were analyzed using a nanoindenter NanoTest automatic platform (Micro Materials Ltd.) equipped with a diamond indenter with a Berkovich pyramidal tip (100 nm diameter) and inside a cabinet with controlled humidity around 40%. 10x10 indentations experiments were performed at 0.5, 1 and 1.5 mN loads with a loading rate of 10 μmN/s and a holding (dwell) time of 30 s at

maximum load that allowed material stabilization prior to unloading. The load-depth curves series show a very good reproducibility, yielding mechanical parameter values with standard deviations below 0.1 % and indicating a high homogeneity down to the micron scale of the polymeric matrices. The relative Young's modulus (E_r) and the hardness (H), were obtained according to the Oliver-Pharr method [16]. The initial slope on the unloading branch (stiffness, S) is related to E_r by

$$S = \left(\frac{dP}{dh}\right)_{h=h_{\max}} = \frac{2\sqrt{\pi}E_r}{\sqrt{A_c}} \qquad (2)$$

where A_c is the area imprinted on the sample. Given the huge Young's modulus difference between the indenter and the sample, and the small values of Poisson's ratio, relative elastic modulus (E_r) can be considered as the elastic modulus ($E_r = E$). The hardness was calculated as the ratio $H = P_{max}/A_{c,}$ where P_{max} is the maximum indentation load. Finally, the elastic recovery, that is, the ratio of recovered depth to the maximum indented depth was also estimated. Indentation depths are selected to be within the effective penetration range of the IR beam to allow a consistent correlation of data provided by both techniques. To prevent artifacts due to non-ideal tip shape and indentation size effects, tip area was carefully calibrated, and different sources of depth-dependence of mechanical properties were taken into consideration [17,18].

The surface texture of samples have been characterized by Atomic Force Microscopy (AFM) (Cervantes, Nanotec Electrónica) using a 10x10 μm^2 scanner and operated in non-contact dynamic mode at the free lever resonance frequency. Images were obtained at room conditions (20-25 °C and 40-50% RH) and processed using the WSxM software [19]. Si_3N_4 rectangular cantilevers with nominal force constant of 2.8 Nm^{-1} and resonance frequency around 80 kHz were used. Parameters such as the

cantilever driving oscillation frequency and amplitude and set point have been carefully selected to operate in the long-range attractive van der Waals forces regime, thus ensuring the minimum perturbation of the sample by the probe. The scanner has been calibrated using a NT-MDT TGT01 silicon grating (2.12 μm pitch) for the X and Y directions, and a Nanosensor H8 certified grating with 7.0 nm step height for the Z direction. Several regions (3-4 per sample) have been analyzed using the maximum scanner range and surface roughness is determined from reproducible areas.

Surface hydrophobicity was analysed by static Water Contact Angle (WCA) measurements at room conditions using an Attension TL100 Optical Tensiometer by the sessile drop method and image profile analysis. A 3 μL Milli-Q grade water drop was deposited in at least 5 different points of every sample and the drop contour was checked for 10 s. In that period, volume losses were less than 1% (evaporation) and contact angle diminished less than 0.7%. WCA values reported correspond to the average of about 20 stable measurements within the first 2 seconds of contact. For surface hydrolysis measurements, the same tensiometer was used and the contour of 4μL drops of pure water and NaOH 1M were compared. In these cases, contour analysis was extended up to 1200 s.

For water permeation experiments, films were mounted in transpiration chambers sealing and contacting the water inside a reservoir. Chambers were introduced in a dry silica desiccator at 22°C and the amount of water transpired was obtained by weighting at regular time intervals. Permeability (P_{wv}) was calculated from the formula:

$$P_{wv} = \frac{J\ l}{S\ \rho\ (a_w - a_{air})} \qquad (3)$$

Where (J) is the transpiration rate obtained from the slope of the linear section of the weight *vs* time curves, (l) is the film thickness, (S) is the film cross-section in contact

with water, (ρ) is the density of the water vapour in saturated air at 22°C and (a_w) and (a_{air}) the water activity at both sides of the film. At least three specimen of each ALE/PAL sample was measured and values averaged. Standard deviations obtained are about ±15%.

For biodegradation tests, polyester films were introduced in nylon net bags and buried in a seed box (250 cm^3) containing standard garden soil (pH=5.5-6.5). Soil moisture was kept constant resembling local pluviometric conditions of 535 mm/year. Sampling times were 20, 40, 60, 90, 120 and 180 days. After that, films were removed and cleaned by sonication in a solution containing 0.25% sodium hypochlorate and 0.1% Tween-85, rinsed with distilled water and dried at room temperature to constant weight. Three replicates per specimen were essayed and degradation rates were obtained from the weight losses observed.

2. Results and discussion

2.1. Bulk chemical characterization

Though this article focuses on the surface characterization of ALE/PAL polyester films prepared by melt-polycondensation in air without using catalysts, for reference purposes, it is necessary to address the chemical characterization of the bulk. Thus, esterification and palmitic incorporation in ALE/PAL polyesters have been studied by ^{1}H and ^{13}C CP-MAS NMR and spectra are plotted in figure 1. Briefly, the presence of palmitic units is indicated by green areas (terminal $–CH_3$ and adjacent $–CH_2$- groups). The formation of the ester is evidenced by signals marked in red while the associated elimination of hydroxyls is highlighted by regions in blue. The most important observations within the series are: (i) most of primary hydroxyls are esterified (peak ~65 ppm) [20,21] and (ii) free secondary hydroxyls (~75 ppm) [22] are progressively

eliminated upon palmitic acid addition. Based on these and on previous NMR and IR results [15] we propose several reactions contributing to such secondary hydroxyl reduction: (i) esterification, caused by the increment of the –COOH/-OH ratio, (ii) dehydration, which is favored in secondary alcohols and (iii) oxidative diol cleavage to form acid groups, figure 2A.

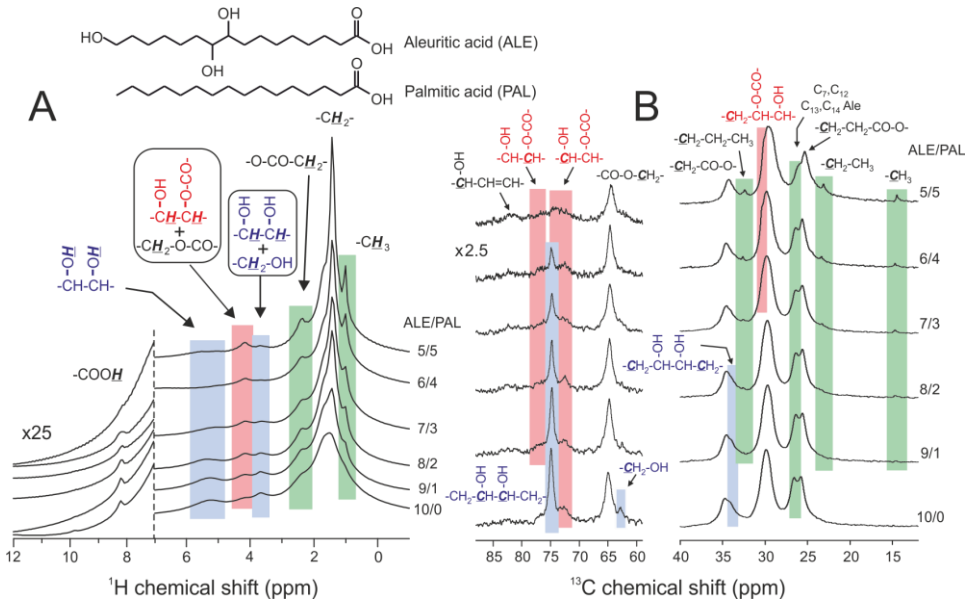

Figure 1. Solid state ^{1}H (A) and ^{13}C (B) CP-MAS NMR spectra of ALE/PAL polyesters. Color code: (green) palmitic incorporation, (blue) esterification reactants and (red) esterification products.

2.2. Reaction kinetics at the near surface region

At the air exposed side of films, esterification can be monitored by the transformation of the carbonyl stretching ν(C=O) of the acid at 1699 cm^{-1} into the one at 1730 cm^{-1} corresponding to an ester, figure 2B (black traces). It is also confirmed by the development of other characteristic ester bands at 1172 cm^{-1} and 1245 cm^{-1} assigned to (OC-O-C) groups [23] (Supporting Information, figure SI1). The main carbonyl ester peak is accompanied by a shoulder around 1710-1717 cm^{-1}, which is due to a series of species comprising hydrogen bonded ester carbonyls (1715 cm^{-1}) [24,25] and –COOH weakly interacting by hydrogen bonding (1710 cm^{-1}) [26,27]. Following this initial

esterification stage, both an increase of the intensity of the carbonyl band (blue traces) and the development of new bands around 1770 cm^{-1}, 1800 cm^{-1} and 1630 cm^{-1} (red traces) are observed. The later one is due to the formation of (C=C) bonds resulting from the alcohol dehydration while those at 1770 cm^{-1} and 1800 cm^{-1} are associated to oxidized species such as acyl peroxides and peroxyesters [28,29,30].

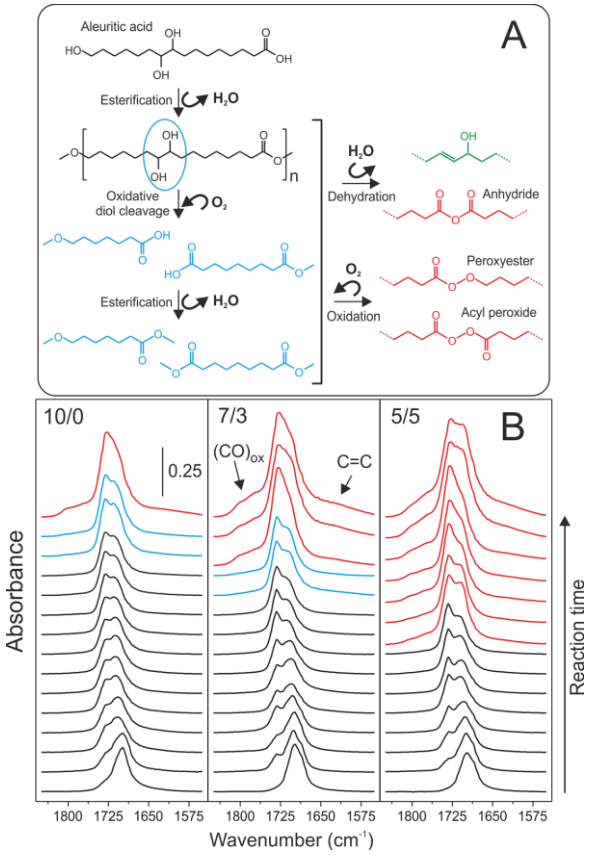

Figure 2. (A) Schematics of reactions detected and (B) $\nu_{C=O}$ ATR-FTIR spectra monitoring the esterification reaction at the air exposed side of films obtained from the indicated aleuritic and palmitic acid mixtures at 150°C. Reaction times are (down to up): 0 (pure acids), 0.5, 1, 1.5, 2, 2.5, 3, 4, 5, 6, 7, 8, 10, 12 and 24 hours. Color code is: (black) esterification stage, (blue) onset of the oxidative diol cleavage and (red) side oxidations and dehydration reactions.

The carbonyl band magnification is better analyzed when areas are calculated and normalized to the ν_{CH} peak of the aliphatic chains, figure 3. The initial flat region of the ($A\nu_{CO}/A\nu_{CH}$) *vs* reaction time plots characterizes the esterification process itself in which acid groups (–COOH) are transformed into esters (-CO-O-) with no carbonyl population modification. At higher reaction times, the ($A\nu_{CO}/A\nu_{CH}$) ratio increases very

noticeably and reaches a saturation value around 1.3-1.4 (saturation is an artifact caused by the limited depth analysis of the single reflection ATR-FTIR technique). Such (Av_{CO}/Av_{CH}) increment is not detected when analyzing the mold facing side of the film (open circles in figure 3 and figure SI2 in Supporting Info) and, consequently, the observed trend is associated with the occurrence of side oxidation reactions when exposed to air. The reaction proposed is the oxidative vicinal diol cleavage and further esterification of the –COOH groups formed. This second esterification stage is consistent with the simultaneous reduction of the hydroxyl population (broad ν_{OH} band around 3400 cm^{-1} in Supporting Info Figure SI1).

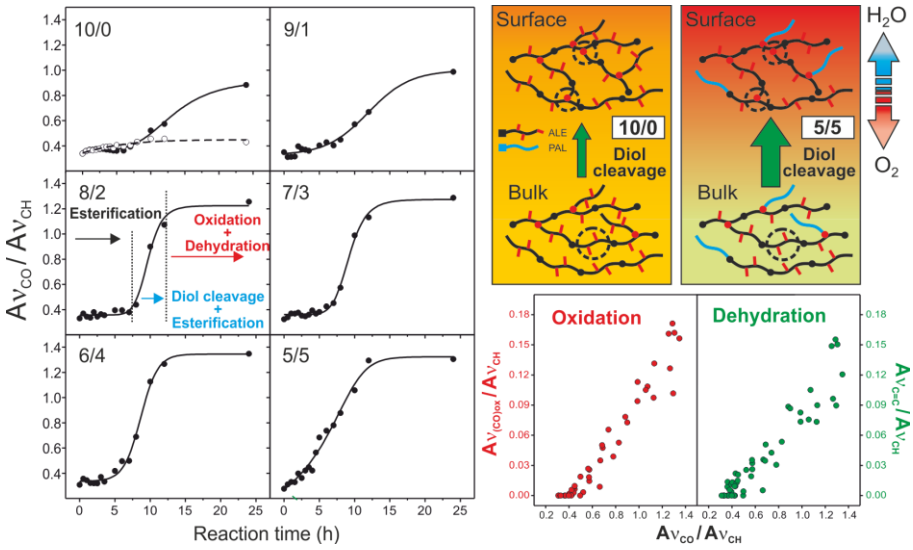

Figure 3. (left) Progression of the normalized $\nu_{(C=O)}$ ATR-FTIR band vs reaction time at the air exposed side of ALE/PAL polyester films (filled circles). As a reference, open circles (dotted line) correspond to the film side in contact with the mold. (bottom-right) Direct relationship between the vicinal diol cleavage progression ($Av_{C=O}/Av_{CH}$) and the production of oxygenated (red) and dehydrated (green) species. (top-right) Schematics of the structural modification induced by the oxidative diol cleavage and further esterification in the 10/0 and 5/5 ALE/PAL network. Color intensity represents the extent of the oxidative processes.

2.3. The effect of palmitic acid addition

The addition of palmitic acid has a strong effect on these chemical processes. As indicated by ATR-FTIR data, esterification, diol cleavage, oxidation and dehydration are evidenced at progressively shorter reaction times. On the other side, dehydration and oxidation processes seem to be associated with the oxidative vicinal diol cleavage

reaction as deduced from the parallelism between the ($Av_{(CO)ox}/Av_{CH}$) and ($Av_{C=C}/Av_{CH}$) *vs* (Av_{CO}/Av_{CH}) plots, figure 3. These three chemical reactions, *i.e.* oxidative cleavage, dehydration and carbonyl oxidation, share no common mechanism explaining their observed interdependence so we propose the diffusion of reactive species or products as the rate limiting step.

2.4. Depth Analysis

To support this hypothesis variable depth ATR-FTIR measurements have been carried out and normalized band areas corresponding to oxidative cleavage, oxidation and dehydration are shown in figure 4 (ATR-FTIR spectra can be seen in Supporting Information figure SI3). As expected, profiles show that side reactions are more intense at the near surface regions and progressively diminish towards the bulk. Also, the air exposed side of the film (figure 4A) is more altered than the face in contact with the mold (figure 4B), particularly by processes requesting oxygen. However, dehydration levels in both sides are similar. These results indicate that the mold behave as a pressure valve allowing the release of water molecules from the bulk but impeding the access of oxygen to the surface. When comparing the ALE/PAL 10/0 and 5/5 samples, it becomes evident that the addition of palmitic acid favors both oxidative and dehydration reactions. Under the preparation conditions used the altered crust is estimated to be about 5µm thick.

2.5.Mechanical characterization

Near surface mechanical characterization has been performed by indentation at several depths within the altered layer of the ALE/PAL 10/0 and 5/5 samples, figure 5. The different mechanical performance of both films is apparent from the load-depth curves and elastic modulus, elastic recovery and hardness values. As observed, the

external layer (below 6 µm) of the ALE/PAL 5/5 sample is stiffer than the ALE/PAL 10/0 one. In both cases, mechanical parameters decay with indentation depth and evolve towards bulk values (table 1) considering that values obtained by the Oliver-Pharr method can be several times higher than those obtained by tensile experiments due viscoelastic and pileup effects in the indentation [31].

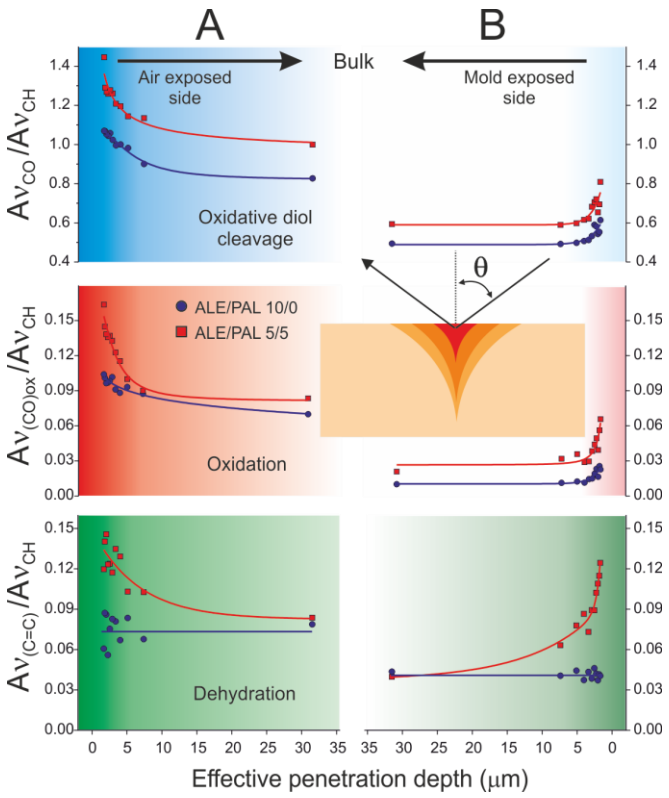

Figure 4. Variable angle ATR-FTIR data showing the concentration depth profiles of species generated in the oxidative diol cleavage (blue), oxidation and peroxidation (red) and dehydration (green) reactions for the 10/0 and 5/5 ALE/PAL polyesters. Profiles are represented from the air exposed side (A) and the mold facing side (B) towards the bulk. The graphical representation of the variable angle ATR-FTIR experiment is inserted.

Though the dependence of the mechanical parameters on the indentation size in polymers it is a well-known phenomenon, physical contributions like adhesion, pressure dependence behavior, higher order displacement effects and confined molecular motion in the interfacial region are reported to be relevant mostly at the submicron range

[18,32]. In our case, these contributions can be neglected considering both the indentation depth achieved and the magnitude of the modifications observed.

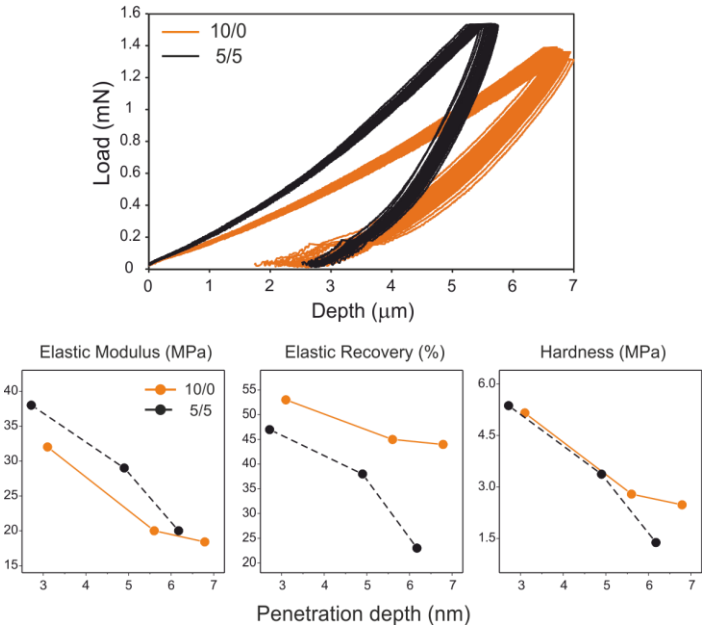

Figure 5. Typical load-depth indentation curves and mechanical parameters obtained as a function of the indentation depth for the air exposed side of the10/0 and the 5/5 ALE/PAL polyesters.

2.6. Textural analysis

Surface texture of the air exposed side of the films has been analyzed by SEM and images obtained (Supporting Info Figure SI4) revealed quite smooth surfaces. The textural analysis was completed by AFM (figure 6) and surface roughness values are quite low (RMS from 0.4 nm to 1.3 nm), but they show a growing trend with the palmitic acid addition.

AFM analysis has been complemented with N_2 adsorption isotherms. S_{BET} values obtained (table in figure 6) are very low, as reported for non-porous polymers [33] and prevents the definition of a clear trend. Further microporosity analysis using CO_2 adsorption at 274 K has been unfruitful because of the very low surface affinity for

CO_2. Thus, and based mostly on AFM results, the overall conclusion is that the addition of palmitic acid causes an increment of the accessible area.

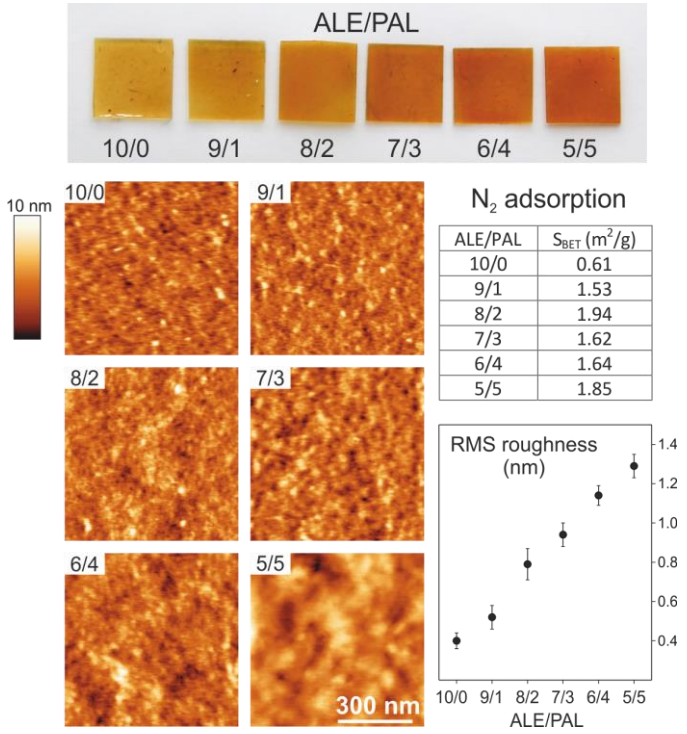

Figure 6. Appearance and textural AFM images of the air exposed side of poly ALE/PAL films. Surface RMS roughness is correlated with the PAL content.

2.7. Surface hydrophobicity and water permeability

Surface affinity for water of the air exposed side of ALE/PAL polyester films has been evaluated by means of static water contact angle measurements (WCA), figure 7A. Two situations have been considered: before and after severe oxidation and diol cleavage conditions (after 8h and 24h reaction, blue and red dots, respectively). In the absence of oxidation, the high WCA values observed (105-102°) show the hydrophobic character of these polyesters. Nevertheless, one may expect the WCA to increase with the PAL content as the result of both: (i) the progressive hydroxyl diminishment and (ii) the increment of surface roughness, however, a decreasing trend is detected. On the other side, it can be observed that hydrophobicity decreases in the same sense as the

oxidative diol cleavage reaction is enhanced, *i.e.* at higher palmitic content and longer reaction time. To investigate such relationship and to highlight the surface chemical modifications involved, the ATR-FTIR spectrum corresponding to a pristine polyester (this is, the one obtained for the 10/0 sample after 8h reaction) has been subtracted from those of the 8h and 24h series. Results are included in figure 7B. As observed, the generation of oxidized, and particularly –COOH, species can be correlated with the WCA decrease. Thus, we conclude that these new species may act as hydrophilic moieties increasing the surface water affinity of ALE/PAL polyesters prepared at longer reaction times and higher PAL content.

On the other side, water permeability values (P_{wv}) show no modification with the PAL content (table 1) and values are similar to those of synthetic polymers like ethylcellulose (EC) and cellulose acetate (CA) [34].

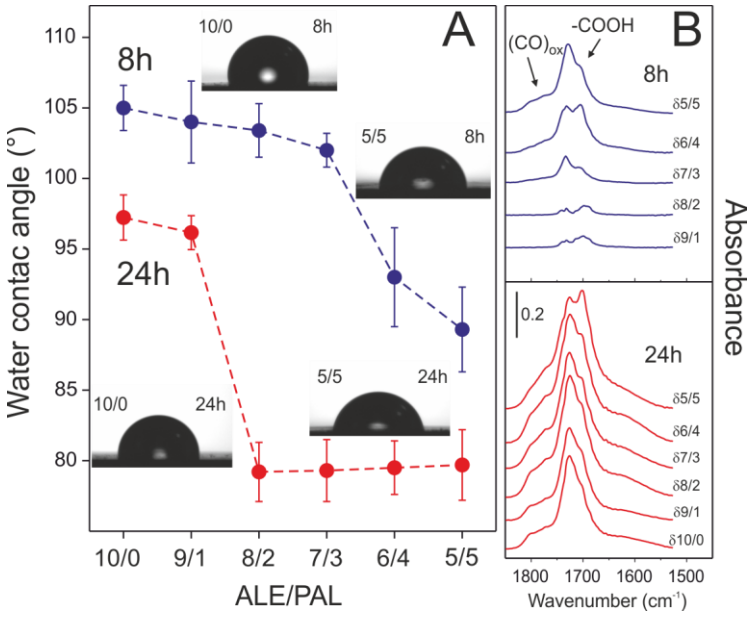

Figure 7. (A) Static water contact angle (WCA) values for the air exposed side of ALE/PAL polyesters prepared before (8h, blue) and after oxidation (24h, red). (B) ATR-FTIR difference spectra remarking the near surface chemical modifications in both series.

2.8. Surface resistance to hydrolysis.

The chemical resistance of the surface of ALE/PAL polyesters towards alkaline hydrolysis has been qualitative determined by placing a drop of a 1M NaOH solution and monitoring the penetration rate, figure 8. To isolate the chemical process from physical contributions like absorption and evaporation of the solvent, the drop volume modification is compared to the one observed for pure water. In these conditions, the relative volume modification of the drop is related to ester linkage hydrolysis and monomer/oligomer migration towards the liquid phase. As observed in figure 8, the volume loss is more intense as the amount of palmitic added is higher. The slopes of the curves at the straight initial regions are compiled in table 1, and, if considered as representative for the reaction rate, it is concluded that surface alkaline hydrolysis is proportional to the palmitic content.

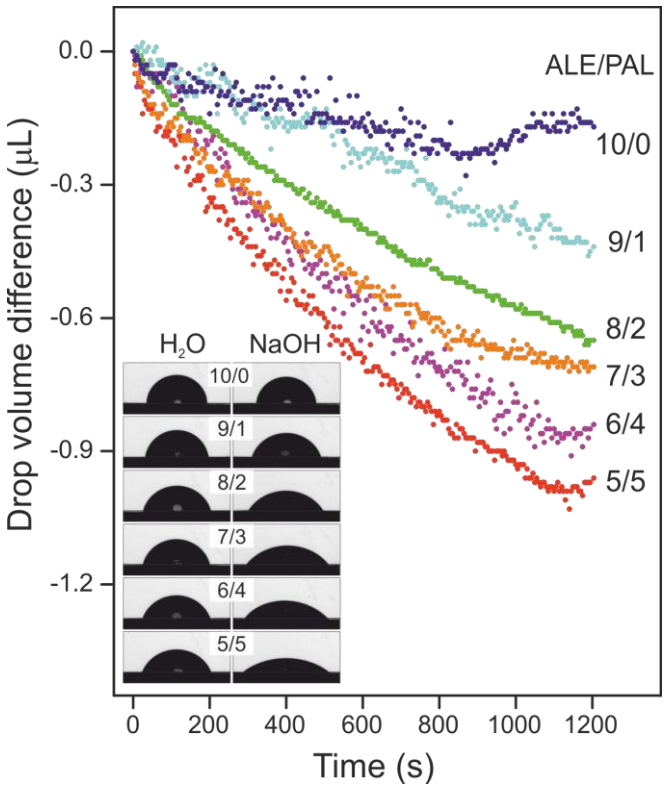

Figure 8. Evolution of water and NaOH solution drops on the surface of the air exposed side of ALE/PAL polyesters. Curves represent the volume difference between the NaOH 1M and the water drops as a function of contact time.

2.9. Biodegradation.

The degradation of ALE/PAL polyesters in contact with soil has been studied for up to 180 days. The weight losses observed are proportional to the contact time and the calculated degradation rates are listed in table 1. As observed, the addition of palmitic acid slows down the process to the point that the time required for a 50% weight loss ($t_{1/2}$) is almost 60 times higher for the 5/5 ALE/PAL film when compared to the 10/0 ALE/PAL. SEM images also reveal important differences, figure 9. The mold side of the films shows a much higher degradation and proliferation of microorganisms than the air exposed side. Fungi hifes and bacteria are clearly visible and, particularly, *Penicillium simplicissimum* and *Fusarium solani* have been isolated and identified as the main microorganisms involved in the biodegradation of these polymers. In both sides, proliferation is reduced as palmitic content is increased. ATR-FTIR spectra reveal the presence of carboxylate species (1644 and 1548 cm^{-1}) resulting from the ester bond cleavage.

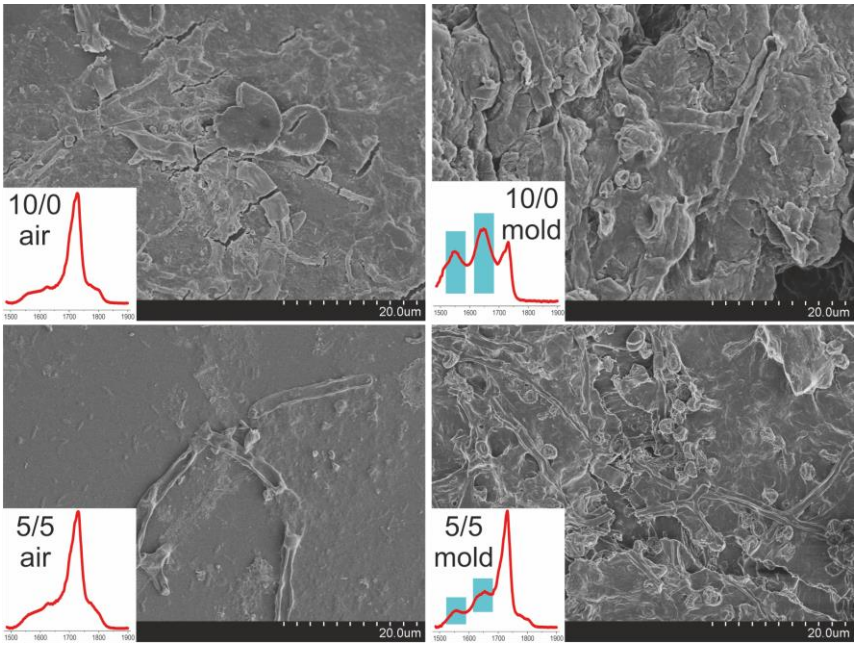

Figure 9. SEM images of both sides of 10/0 and 5/5 ALE/PAL films after degradation in contact with soil for 40 days. $\nu_{C=O}$ ATR-FTIR spectra are included.

3. Discussion

To prevent side reactions affecting their structure and properties, polyesters are generally synthesized under an inert atmosphere. It is also very common the use of a reduced pressure to favor the release of the water molecule and to improve the reaction yield. In the presence of oxygen, the melt-polycondensation reaction becomes uncontrollable and low molecular weight polymers with unsatisfactory properties are usually obtained. One of the most evident signs of oxidation is the yellowing of the polyester which may be considered artistically unpleasant. ALE/PAL polyesters prepared here display such yellow to light brown coloring. However, when applied as a few microns thick coating, the result is a nice golden finish comparable to those observed in commercial food cans. On the other side, the advantages of a direct synthesis, as the one reported here, in terms of simplicity and cost reduction is worth being considered. Additionally, partial oxidation can be envisaged as a tool to intentionally modify the structure of polymers. Thus, the oxidative degradation has been proposed as a feasible method to transform microbial polyesters into copolymers without any additional agents such as solvents or catalysts [35]. Analogously, the following paragraphs will discuss and evaluate the role of oxygen in inducing side reaction and in positively modifying the properties of the near surface region of the ALE/PAL polyesters.

^{1}H and ^{13}C CP-MAS NMR results show that the esterification of aleuritic acid in these experimental conditions mainly involve primary hydroxyls. The structure of the ALE polyester can then be described as mostly linear; with some degree of branching due to the partial esterification of secondary hydroxyls. This primary skeleton is completed with a secondary network of hydrogen bonded hydroxyls, scheme in figure 3. Blocking of primary and secondary hydroxyls upon palmitic acid (PAL) addition

reduces chain propagation, branching and hydrogen bonding. Such chain size diminution is likely the cause of the decrease of the bulk tensile parameters and the insoluble fraction, as well as the increment of the hydrolysis rate, table 1. However, no cross-linking by ester bonding is formally possible in any of the ALE/PAL formulations because there is only one –COOH group per monomer.

ATR-FTIR data have shown the occurrence of side reactions caused by oxygen along the synthesis of the polyester, particularly the oxidative cleavage of vicinal hydroxyl groups. The subsequent esterification of the new –COOH groups formed has a direct effect in the architecture of the polymer. Thus, the creation of two ester bonds per broken C-C linkage results in chain crosslinking and in the reinforcement of the structure (scheme in figure 3). In this mechanism, crosslinking requests both the access of oxygen to initiate the oxidative cleavage and the release of water resulting from intra-esterification. ATR-FTIR depth analysis has stated that the addition of palmitic acid enhances oxygen and water diffusion across the polymer matrix reaching deeper regions in a shorter time. Such enhancement of O_2 and H_2O diffusion at the near surface region is likely caused by both the increment of the accessible surface area and the definition of more effective pathways through the ALE/PAL network. Consequently, crosslinking is expected to be incremented at the near surface regions of the palmitic added samples.

Indentation results corroborate these hypotheses. Data suggest a more reduced alteration layer in the ALE/PAL 10/0 specimen as values stabilize below 5-6 μm while no such stabilization is observed for the ALE/PAL 5/5 sample. Compared to the ALE/PAL 10/0, the higher elastic modulus and lower elastic recovery of the ALE/PAL 5/5 sample is consistent with a more crosslinked surface region [36]. On the other side, the higher hardness decrease in the ALE/PAL 5/5 sample is related to the diminution of

the secondary hydrogen bonded hydroxyl network and implies a lower capacity of resistance to permanent plastic deformation.

Cross-linking also influences the surface degradation by alkaline hydrolysis of ALE/PAL films. If such degradability is related to the possibility of scission of monomers or oligomers from the polymer network, the reduction of chain size caused by PAL addition accounts for the fast growing of bulk hydrolysis rates (table 1). However, if the ALE/PAL structure at the surface is reinforced by additional ester bonds, the probability of scission decreases and justifies the smoother hydrolysis rate trends observed at the surface of films when compared to those of bulk.

Affinity for water of bulk ALE/PAL polyesters is found to depend on the availability of free hydroxyl groups (table 1). For this reason, both the reduction of the ALE fraction and the hydroxyl consumption in the oxidative cleavage were expected to cause an increment of surface hydrophobicity upon PAL addition. However, experimental results showed the opposite behavior. Meanwhile, ATR-FTIR revealed the development of a residual free –COOH surface phase, figure 7. The growing concentration of such acid phase in PAL rich specimen is likely due to the combination of two interconnected factors: (i) the enhancement of the oxidative cleavage originated by a better diffusion of oxygen and (ii) the reduction of the probability of ester formation by the associated fast hydroxyl depletion. Thus, the reduction of WCA values is caused by the presence of surface hydrophilic –COOH centers surpassing the effect of both the reduction of hydroxyls and the increment of surface roughness. Despite this unfavorable result, still WCA values obtained are similar to those of common packaging materials like PET, PVDC, PVC and PS. Conversely, water permeability of ALE/PAL polyesters is two to three orders of magnitude higher [33,37]. In any case, ALE/PAL polyesters show an acceptable water barrier capacity.

Finally, when biodegradation in contact with soil and alkaline hydrolysis data are compared, opposite trends are observed, table 1. This is an indication that in ALE/PAL polyesters, biodegradation is mostly carried out by the action of microorganism rather than to a mere hydrolysis chemical reaction with soil. Microorganism fixation and activity on the surface of a film are conditioned by many factors such as texture, chemical composition and wettability. Though, surface roughness and hydrophilicity increases by the addition of palmitic acid in ALE/PAL polyesters, microorganism proliferation diminishes, figure 9. Consequently, fungal activity is mainly related to the chemical modification induced by the additive and the preparation method. The formation of the oxidized surface layer reduces biodegradation and becomes a variable to adjust the antimicrobial activity of these polyesters.

Biodegradation of polyhydroxyalkanoates in contact with soil strongly depend on conditions facilitating the proliferation of microorganisms such as the substrate chemical composition, temperature, humidity and availability of oxygen [38,39,40]. This complicates result comparison from different sources, but, as a reference, half-life times obtained here are very similar or even shorter than those reported for PHB and PHV copolymers in wet fertilized substrates ($t_{1/2}$ = 15-105 days).

4. Conclusions

Bulk and surface physical and chemical properties of aleuritic/palmitic (ALE/PAL) polyesters films prepared by melt-polycondensation in air at 150°C without using catalysts are found to differ. While bulk parameters are controlled by the reduction of both chain size and free hydroxyls availability upon palmitic acid addition, surface behavior is conditioned by chemical and structural modifications caused by a series of oxidative processes. The most important is the oxidative diol cleavage and further

esterification of aleuritic units that give rise to chain cross-linking. Such cross-linking improves both the surface mechanical performance and the resistance to alkaline hydrolysis when compared to bulk. Though the chemical modification caused by such oxidative cleavage significantly reduces an important feature like surface hydrophobicity, it is also responsible for the enhanced antimicrobial activity of ALE/PAL polyesters. Therefore, the characterization of surface parameters is of key importance in the application of such polyesters as barrier films or coatings if prepared directly in air by melt-polycondensation.

Acknowledgments

Funding is provided by the Spanish Ministerio de Economía y Competitividad, project CTQ2011-24299, and by Junta de Andalucía grant TEP-7418. JAH-G acknowledges the BIOPROTO project (Marie Curie Intra-European Fellowship), financed by the EU Seventh Framework Programme for Research (FP7). VM-F would like to thank the support from the IV Plan Propio de Investigación, from the Universidad de Sevilla. MAC-C is grant holder from the CONACYT (Mexico) mobility program.

Table 1. Physical and chemical parameters of ALE/PAL polyesters

ALE/PAL (mol/mol)	X_P[a]	Insoluble fraction[b] (%)	Young´s Modulus (MPa)	UTS (MPa)	Specific water uptake[c] (mol g^{-1} $x10^4$)	Water permeability (m^2 s^{-1} $x10^8$)	Hydrolysis rate (bulk)[d] (%w/w h^{-1})	Hydrolysis rate (surface)[e] (µL s^{-1} $x10^4$)	Biodegradation rate (%w/w d^{-1})	Biodegradation half-life time ($t_{1/2}$) (days)
10/0	0	94	3.9	1.2	2.07	6.2	0.4	2.1	0.70	72
9/1	0.10	90	2.8	0.9	1.60	6.0	0.5	3.9	0.48	104
8/2	0.15	82	3.3	1.1	1.38	7.2	0.7	5.6	0.35	143
7/3	0.20	82	3.0	0.8	1.04	6.4	0.9	7.3	0.24	211
6/4	0.23	82	3.3	0.9	0.97	6.0	1.5	9.2	0.11	467
5/5	0.27	70	1.4	0.2	0.57	7.1	3.6	10.1	0.01	4167

[a] From quantitative ^{13}C NMR

[b] In DMSO at 100°C for 24h

[c] From DSC after 48h at 50% RH

[d] Gravimetrically at RT in NaOH 0.25M

[e] Tensiometer, 4µL NaOH 1M drop at RT

References

[1] Kolattukudy P E 2001 Advances in Biochemical Engineering/Biotechnology *Biopolyesters* (Berlin Heidelberg: Springer-Verlag) **71** 1-49

[2] Schreiber L 2010 *Trends Plant Sci.* **15** 546-553

[3] Gandini A, Pascoal Neto C and Silvestre A J D 2006 *Prog. Polym. Sci.* **31** 878-892

[4] Olsson A, Lindstrom M and Iversen T 2007 *Biomacromolecules* **8** 757-760

[5] Heredia-Guerrero J A, Heredia A, García-Segura R and Benítez J J 2009 *Polymer* **50** 5633-5637

[6] Sousa *et al* 2011 *J. Polym. Sci. Part A: Polym. Chem.* **49** 2281-2291

[7] Gómez-Patiño M B *et al* 2015 *Frontiers in Materials* **2** 67

[8] Garcia H *et al* 2014 *Biomacromolecules* **15** 1806-1813

[9] Benítez J J *et al* 2015 *Frontiers in Materials* **2** 59

[10] Baker E A and Holloway P J 1970 *Phytochemistry* **9** 1557-1562

[11] Walton T J and Kolattukudy P E 1972 *Biochemistry* **11** 1885-1897

[12] Santos S A, Cotter J F and McWeeney M M 202 US Patent 6,348,217

[13] Berger S and Sicker D 2009 Isolation and Structure Elucidation of Natural Products *Classics in Spectroscopy* (Weinheim: Wiley-VCH Verlag GmbH & Co) 519-538

[14] Benítez J J *et al* 2015 *J. Appl. Polym. Sci.* **132** 41328

[15] Benítez J J *et al* 2015 *Soft Materials* **13** 5-11

[16] Oliver W C and Pharr G M 1992 *J. Mater. Res.* **7** 1564-1583

[17] Briscoe B, Fiori L and Pelillo E 1998 *J. Phys D: Appl Phys* **31** 2395-2405

[18] Alisafaei F and Han C 2015 *Adv Condens Mat Phys* **391579** 1-20

[19] Horcas I *et al* 2007 *Rev. Sci. Instrum.* **78** 013705

[20] Liu C *et al* 2011 *Biomacromolecules* **12** 3291-3298

[21] Deshmukh A P, Simpson A J and Hatcher P G 2003 *Phytochemistry* **64** 1163-1170

[22] Pandey A K, Nande S S, Selukar B S and Garnaik B 2010 *e-Polymers* **131** 1-12

[23] Bellamy L J 1975 *The Infrared Spectra of Complex Molecules*, vol. 1 (London: Chapman and Hall) 203-205

[24] Ramirez F J, Luque P, Heredia A and Bukovac M J 1992 *Biopolymers* **32** 1425-1429

[25] Heredia-Guerrero J A et al 2014 Frontiers in Plant Sci. 5 1-14

[26] Maréchal Y and Chamel A 1996 *J. Phys. Chem.* **100** 8551-8555

[27] Dong J, Ozaki Y and Nakashima K 1997 *Macromolecules* **30** 1111-1117

[28] Davison W H T 1951 *J. Chem. Soc.* 2456-2461

[29] Yin H., Hachey D L and Porter N A 2001 *J. Am. Soc. Mass Spectrom.* **12** 449-455

[30] Peng H, Alemany L B, Margrave J. L and Khabashesku V N 2003 *J. Am. Chem. Soc.* **125** 15174-15182

[31] Tranchida D, Piccarolo S, Loos J and Alexeev A 2006 *Appl. Phys. Lett.* **89** 171905

[32] Tweedie C *et al* 2007 *Adv. Mater.* 19 2540-2546

[33] Zaleski R, Stefaniak W, Maciejewska M and Goworek J 2009 *J. Porous Mater.* **16** 691-698

[34] Schreiber L and Schönherr J 2009 *Water and Solute Permeability of Plant Cuticles* (Berlin Heidelberg: Springer-Verlag) 63

[35] Michalak M, Kwiecien M, Kawalec M and Kurcok P 2016 *RSC Adv.* **6** 12809

[36] Jiang C *et al* 2007 *Adv. Funct. Mater.* **17** 2229–2237

[37] Lange J and Wyser Y 2003 *Packag. Technol. Sci.* **16** 149-158

[38] Nishide H, Toyota K and Kimura M 1999 *Soil Sci. Plant Nutrition* **45** 963-972

[39] Matavulj M and Molitoris H P 2000 *Hoppea, Denkschr. Regensb. Bot. Ges.* **61** 735-749

[40] Shogren R L *et al* 2003 *Polym. Degrad. Stab.* **79** 405-411